ELECTRICAL IMPEDANCE TOMOGRAPHY ALGORITHM USING SIMULATED ANNEALING AS A SEARCH METHOD

Claudia Natalia Lara Herrera, natylara@gmail.com
Miguel Fernando Montoya Vallejo, montovall@gmail.com
Fernando Silva de Moura, fernandosmoura@gmail.com
Julio Cesar Ceballos Aya, jccaya@gmail.com
Raul Gonzalez Lima, lima.raul@gmail.com
Department of Mechanical Engineering - Polytechnic School of University of São Paulo Av. Prof. Mello Morães, 2231 - São Paulo - SP - 05508-900, Brazil

Abstract. *Electrical impedance tomography (EIT) is a noninvasive monitoring technique to produce images that represent the cross-sectional distribution of the electrical resistivity within an object (for instance the human thorax) from measurements on its boundary. Mathematically, the absolute resistivity distribution estimation is a nonlinear ill-posed inverse problem. This paper presents a probabilistic reconstruction algorithm based on Simulated annealing method for the solution of the absolute EIT inverse problem. The advantage of this algorithm is that no evaluation of function derivatives is needed and it has the possibility to escape from local minimum. This work contributes to the development of image estimation algorithms applied to monitor mechanical ventilation of lungs. Using simulated data, the localization of object, the size of object and the resistivity of the object are well inside the accuracy of EIT obtained by classical methods. However, using experimental data, the spatial resolution of the object is not good. Only a box restriction of the solution space were imposed. A regularization technique is necessary to obtain images with higher spatial resolution. In both, numerically simulated and experimental tests, the computational effort is large. This results show feasibility of the proposed algorithm.*

Keywords: *Electrical Impedance Tomography, simulated annealing, inverse problems, finite elements method*

1. INTRODUCTION

Electrical Impedance Tomography (EIT) is a noninvasive technique used to produce images that represent the cross-sectional electrical resistivity distribution (or conductivity) within a domain (for instance the human thorax) from electrical measurements made through electrodes distributed on its boundary. A low amplitude alternated electrical current is applied by two or more electrodes with a constant intensity and the difference of electrical potential generated (voltage) is measured in all the rest of the electrodes equally spaced. The way of injecting currents and reading electrical potentials are called *current patterns* and *electrical potential patterns*, respectively. The pair of electrodes used in the current injection is changed successively until enough number of observations allows the estimation of an image. The image is the resistivity distribution with Maximum a Posteriori Probabilityon.

EIT is an innovative monitoring tool for applications in the fields of medicine, geophysical, environmental science and non-destructive materials tests. Some examples of medical applications of the EIT are the detection of pulmonary embolism [2, 3, 4], monitoring of apnea [5], monitoring of brain function [6], monitoring of heart function and blood flow [7] and the detection of breast cancer [8].

It is a noninvasive technique without collateral effect. The cost of the electronic hardware is relatively unexpensive. No radiation is used and the equipment is portable. The drawback of this technique is its low spatial resolution, which is related with the number of used electrodes.

The Resistivity distribution search can be made with the aid of models that depend or not on the time, generating *static* or *dynamic* methods. The static methods are used when the electrical properties of the domain do not vary significantly during the time necessary for data collection. When faster changes of the electrical properties happen, the dynamic effects must be taken into account, a dynamic method must be used. EIT methods can further classified: *difference* imaging and *absolute* imaging. In difference imaging two electrical potentials data sets are measured corresponding to two different target resistivity distributions. Based on the difference between these measurements, the difference of the resistivity distributions can be estimated. In absolute imaging the estimation is based on a single data set of electrical potential measurements, and the aim is to estimate the absolute resistivity distribution.

On the other hand, the problem of EIT is seriously complicated by the non-linearity of the governing equation. Only boundary measurements are available. The EIT inverse problem is ill-posed and ill-conditioned. The boundary measurements are relatively insensitive to changes of resisitivity near the center of the domain. Some *regularization techniques* are required. These techniques allow the inclusion of *prior* information, which is known information about the resistivity distribution in the domain.

An EIT system has hardware to apply currents and then measure electrical potential and software to estimate resistivity images. The estimation problem is divided in two parts [11, 12]. The first part, the *forward problem* of EIT consists of

modeling boundary electrical data as an explicit function of the resistivity (or conductivity) in the domain. The second part, the *inverse problem* of EIT consists of computing the internal resistivity distribution from boundary electrical data.

Approaches to solve the inverse problem for reconstruction of EIT fall into several categories like: the *non-iterative* methods that are frequently used to obtain difference images, are fast, have low computational cost and lead to inexact results [1, 13, 14]; the *iterative* methods that consider the nonlinear relation that exists between the electrical potentials and electrical resistivity, are promising for obtaining more accurate results and have high computational cost. The iterative solutions generally follow similar categories [15, 16, 17].

The present work evaluates the performance of a probabilistic algorithm based on the Simulated Annealing method (SA) to obtain absolute resistivity distributions in a 2-D domain. The SA differs from the traditional search methods, no evaluation of objective function derivatives is needed and has the possibility to escape from a local minimum through the use of Metropolis criterion for acceptance of new points in the search space. The developed algorithm solves the inverse problem of EIT by solving direct problems. The search is accomplished by the metropolis algorithm [18]. It is assumed that the random image that minimizes an index, which is a function of the difference between the measured electrical potential on the boundary and calculated electrical potential, is the closest to the distribution of real resistivity. This makes the method especially attractive when the index to be extremized present multiple local minimum [19]. The SA allows to use restrictions on the solution space.

The next sections of the paper are organized as follow. Section 2 shows the mathematical governing equations of EIT. In section 3 is briefly explained how the domain is modeled using FEM. Section 4 describes in more details the Simulated Annealing method and its formulation for the application in EIT. The methodology of performed tests and its results are shown in section 4 and section 5, respectively. Finally, section 6 draws the conclusions.

2. MATHEMATICAL MODEL OF THE DOMAIN AND ELECTRODES

The domain is considered a bi-dimensional region closed $\mathbf{\Omega}$ and limited by a contour surface $\partial\mathbf{\Omega}$. The resultant electrostatic field is governed by the Maxwell's equations. To reduce the complexity of the EIT problem some simplifying hypotheses must be adopted. If the domain is related to a body section, Poisson's equation can be used to represent the electrical potential $\boldsymbol{\phi}(x, y)$ inside of $\mathbf{\Omega}$.

$$\nabla \cdot (\boldsymbol{\sigma} \nabla \boldsymbol{\phi}) = 0 \tag{1}$$

To limit the infinite number of solutions $\boldsymbol{\phi}(x, y)$ of Eq. (1), boundary conditions are applied on $\partial\mathbf{\Omega}$. In EIT the electrical potential measurements and injection currents are made through l electrodes fixed on certain points of $\partial\mathbf{\Omega}$, thus, the following boundary conditions can be stated

$$\boldsymbol{\sigma} \frac{\partial \boldsymbol{\phi}(\boldsymbol{\sigma})}{\partial \hat{\boldsymbol{n}}} = \begin{cases} J_i, & i = 1, 2, \cdots, l \\ 0, & \text{in the other points of } \partial\mathbf{\Omega} \end{cases} \tag{2}$$

where$\hat{\boldsymbol{n}}$ is an outward normal vector to $\partial\mathbf{\Omega}$. The Eq. (1) is a complex nonlinear partial differential equation, such that it is impossible to get a general analytic solution for an arbitrary resistivity distribution and irregular boundary shape. Therefore, numerical techniques are indicated. The Finite Elements Method (FEM) is a well accepted and powerful numerical method to solve the forward EIT problem.

To model the whole domain $\mathbf{\Omega}$ it is necessary modeling the interaction of the electrodes in $\partial\mathbf{\Omega}$ too. The complete electrode model takes into account both the shunting effect of the electrode and the contact impedance between the electrodes and the domain. Additionally to Eq. (1), electrode model equations are stated

$$\int_{\partial\mathbf{\Omega}_j} \boldsymbol{\sigma} \frac{\partial \boldsymbol{\phi}}{\partial \hat{\boldsymbol{n}}} = I_j, \qquad j = 1, 2, \cdots, l \tag{3}$$

$$\boldsymbol{\sigma} \frac{\partial \boldsymbol{\phi}}{\partial \hat{\boldsymbol{n}}} = 0, \tag{4}$$

$$\boldsymbol{\phi} + z_j \, \boldsymbol{\sigma} \frac{\partial \boldsymbol{\phi}}{\partial \hat{\boldsymbol{n}}} = V_j, \qquad j = 1, 2, \cdots, l \tag{5}$$

where I_j in Eq. (3) represents the electrical current that flow through the j^{th} electrode. In Eq. (5) z_j is the effective contact impedance between the j^{th} electrode and medium and $\boldsymbol{V}$ is the electrical potential in the electrodes.

3. USE OF FEM IN EIT

An inverse problem can be solved iteratively using the solution of its corresponding forward problem. In the particular case of EIT a model that predicts the internal electrical potential distribution given the electrical current excitation and the internal resistivity distribution of the domain must be adopted, known as forward problem. We use the FEM to discretize the domain, including the electrodes.

The finite elements meshes used to divide $\mathbf{\Omega}$ have m nodes and n triangular plain finite elements with constant resistivity ρ_i, $i = 1, 2, \cdots, n$ and linear interpolation functions [11]. The domain is discretized in such a way that regions experimenting high modification in the resistivity have smaller elements. Refined meshes in this way lead to more accurate models. The domain is divided in FE by using the mesh generation software

The matrix $\tilde{\boldsymbol{Y}}_i(\rho_i^{-1}) \in \mathbb{R}^{3\times3}$ is denominated *local conductivity matrix* of the i^{th} element. Considering e the element height, $\mathbb{A}_i$ the element area and the resistivity being homogeneous and isotropic the components of the local resistivity matrix are given by

$$[\tilde{\boldsymbol{Y}}_i(\rho_i^{-1}]_{(k,m)} = \frac{e\rho_i^{-1}}{4\mathbb{A}_i}\left(\xi_k\,\xi_m + \tau_k\,\tau_m\right) \qquad (k, m = 1, 2, 3) \tag{6}$$

with

$$\begin{aligned} \xi_1 &= (y_2 - y_3) \;\;,\;\; \tau_1 = (x_3 - x_2) \\ \xi_2 &= (y_3 - y_1) \;\;,\;\; \tau_2 = (x_1 - x_3) \\ \xi_3 &= (y_1 - y_2) \;\;,\;\; \tau_3 = (x_2 - x_1) \end{aligned} \tag{7}$$

The electrodes are discretized in 2-D finite elements following the work of Hua [20], in which are solved Eq. (3), Eq. (4) and Eq. (5) with the aid of the FEM. Electrode model take into account the low metal resistivity and the contact impedance between metal and medium. The interface between the electrode and medium is discretized using two quadrangular finite elements with 6 nodes in total. To determine the *local conductivity matrix of the electrode* it is followed the same procedure used to find the local conductivity matrix of the elements of $\mathbf{\Omega}$ then

$$\tilde{\boldsymbol{Y}}_j^{\,e} = \frac{b\,\rho_j^{-1}}{t}\begin{bmatrix} \frac{a}{2} & 0 & 0 & \frac{-a}{2} \\ & a & 0 & -a \\ \boldsymbol{sim} & & \frac{a}{2} & \frac{-a}{2} \\ & & & 2a \end{bmatrix} \tag{8}$$

where a is element width, t is the thickness of contact interface and b is the interface thickness (perpendicular to a and t).

It is defined

$$z_j = \frac{\rho_{j^{-1}}}{t} \tag{9}$$

as the effective contact impedance in $[\Omega m^2]^{-1}$. The matrix $\bar{\boldsymbol{Y}}_j^{\,e}$ represents the local conductivity matrix of the electrode written in terms of global coordinates. Then, the summation of all local matrices of the elements and the electrodes is equivalent to the application of the variational principle in the discretized domain [22] and the global conductivity matrix $\boldsymbol{Y}(\boldsymbol{\rho}^{-1}) \in \mathbb{R}^{m\times m}$ is determined

$$\boldsymbol{Y}(\boldsymbol{\rho}^{-1}) = \sum_{i=1}^{n}\left[\tilde{\boldsymbol{Y}}_i(\rho_i^{-1})\right] + \sum_{j=1}^{l}\left[\bar{\boldsymbol{Y}}_j^{\,e}(z_j)\right] \tag{10}$$

After assembling the global conductivity matrix (Eq. (10)) we have *m* nodes, *l* electrodes and *n* elements in which *p* currents are injected. Thus, the matrix containing unknown nodal electrical potentials $\boldsymbol{v}(\boldsymbol{\rho}^{-1}) = [\boldsymbol{v_1} \cdots \boldsymbol{v_j} \cdots \boldsymbol{v_p}]$, $\boldsymbol{v_j} \in \mathbb{R}^m$ corresponding to each applied current pattern is solved through the linear system equations given by

$$\boldsymbol{YV} = \boldsymbol{C} \tag{11}$$

where $\boldsymbol{\rho}_p \in \mathbb{R}^{n+l}$ is any particular resistivity distribution for which it is calculated $\boldsymbol{y}$, and $\boldsymbol{c} = [\boldsymbol{c_1} \cdots \boldsymbol{c_j} \cdots \boldsymbol{c_p}]$, $\boldsymbol{c_j} \in \mathbb{R}^m$ is the matrix of linearly independent bipolar current patterns. On numerical simulations and experimental tests $\boldsymbol{c}$ is

$$\boldsymbol{C} = \begin{bmatrix} -I & 0 & \cdots & +I \\ 0 & -I & \cdots & 0 \\ +I & 0 & \cdots & 0 \\ 0 & 0 & \cdots & 0 \\ \vdots & \vdots & \ddots & \vdots \\ 0 & 0 & \cdots & -I \\ 0 & 0 & \cdots & 0 \end{bmatrix} \tag{12}$$

To solve the equation that governs the forward problem, Eq. (11) , it is necessary to eliminate the singularity of matrix $\boldsymbol{Y}$, this can be made by choosing an arbitrary node with null value (ground). The imposition of this boundary condition it is made by equaling to zero the row and column of the matrix $\boldsymbol{Y}$ corresponding to selected node and attributing to the intersection element the unitary value [16].

4. SIMULATED ANNEALING

In 1953, the *Simulated Annealing* (SA) method was first proposed by Metropolis [18]. It is an algorithm for the efficient simulation of the evolution of a solid to thermal equilibrium. In short, the SA algorithm is based on the analogy between the simulation of the annealing of solids and the problem of solving large combinatorial optimization processes [23, 24]. The annealing denotes a thermal cooling process that starts with a crystal in liquid state, at high temperature, followed by the slow and gradual reduction of the temperature until the solidification point is reached when the system achieves a state of "minimal energy". Minimal states of energy are characterized for a structural state of the material undergone to annealing that would not be obtained if the cooling was not gradual. In conditions less careful of cooling the material would be crystallized by an "locally minimal energy", in other words, the atomic structure of the material would be irregular and weak, with some imperfections.

The physical analogy between the annealing of solids and an optimization problem would be the next:

- The system energy $\varepsilon \Leftrightarrow$ objective function F of the optimization problem,
- system state $\Leftrightarrow$ solution of optimization problem,
- current system state $\Leftrightarrow$ candidate solution,
- minimal energy configuration $\Leftrightarrow$ optimal solution,
- the system temperature $T \Leftrightarrow$ control parameter

The central point of the algorithm is focused on the process of probabilistic acceptance of a nearby solution that may represent an increase in F (higher cost). Summarizing, the algorithm is basically characterized by two operations: the first one is the reduction of the value of the control parameter T successively along the iterations based on a determined *annealing function* ; the second one is the realization of the cycle of generation and acceptation of solutions and equivalent to the Metropolis Algorithm, in such a way that the solutions corresponding to the thermal equilibrium be found to each temperature. The algorithm ends when a determined *stopping criterion* is satisfied.

The heuristic parameters should be well adjusted to improve the performance (i.e, efficiency, convergence, speed) as also the efficacy (i.e, quality of the found solutions) of the algorithm. Amongst these parameters are:

- The initial temperature, T_0, must be a value high enough such that all the candidate solutions in the neighborhood (both: the ones which improve and the ones that get worse the objective function) have a probability next to 1 of being chosen.
- It is required to determine a (*cooling schedule*) that defines the evolution of T during an limited number of iterations. In this work the geometric cooling is used, whose general formula is given by

$$T_{k+1} = \alpha T_k \tag{13}$$

  The factor α is a constant next to the unitary value and is the temperature decay rate. The value of the cooling factor α defines the convergence of the SA. If α is sufficiently high, the probability to converge to a global optimal point increases and the computational time increases unnecessarily. The more commonly used values are between 0.9 and 0.99 [25].
- the number of iterations to reach the equilibrium at certain temperature, N_t. The simplest criterion is to make a fixed number of iterations before the temperature is changed.
- the simplest stopping criterion is the pre-definition of the total number of iterations N be executed by the algorithm. However, this criterion needs to be chosen carefully together with the other parameters so that the algorithm reaches sufficiently low temperatures that guarantee the convergence.

4.1 SA and the EIT inverse problem

It is assumed that for the minimization of the objective function, the image, $\boldsymbol{\rho}$, will converge to the requested original image. In that way, the quadratic error between electrical potentials, measured and computed, was chosen as objective function and the problem is described by a nonlinear optimization model,

$$\begin{aligned} &\min_{\boldsymbol{\rho}\in\,\boldsymbol{\Omega}} \quad F(\boldsymbol{\rho}) \\ &F(\boldsymbol{\rho}) = \frac{1}{2}\left\|\boldsymbol{V_m} - \boldsymbol{V_c}(\boldsymbol{\rho})\right\|_2^2 \end{aligned} \tag{14}$$

In EIT it is possible to include additional information in the reconstruction problem. In the present work it was possible to include restrictions in the solution space. This additional information was used. The search covers the entire domain of the impedance distribution restricting the space solution between a limited superior vector and limited inferior vector whose values are defined according prior information about the problem.

The restrictions are imposed to obtain the new candidate point (candidate configuration). New candidate point is generated around the current point applying random moves along each coordinate direction, in turn and satisfying the imposed limits [26]. Let $F(\boldsymbol{\rho})$ be the function to minimize and let $a_1 < \rho_1 < b_1,\ a_2 < \rho_2 < b_2, \ldots,\ a_n < \rho_n < b_n$ be its variables, each ranging in a finite, continuous interval. Therefore, starting from the point $\boldsymbol{\rho}_i$, generate a random point $\boldsymbol{\rho}'$ along the direction h

$$\boldsymbol{\rho}' = \boldsymbol{\rho}_i + r\gamma_h \boldsymbol{\beta}_h \tag{15}$$

where r is a random number generated in the range $[-1, 1]$ by a pseudo-random number generator; $\boldsymbol{\beta_h}$ is the vector of the h^{th} coordinate direction; and γ_h is the component of the step vector $\boldsymbol{\gamma}$ along the same direction.

If the h^{th} coordinate of $\boldsymbol{\rho}'$ lies outside the limits, that is, if $\rho'_h < a_h$ or $\rho'_h > b_h$, then a new random point in this direction must to be generated. With this, it is guaranteed the probability of accepting a new point that is out of the imposed limits is null and that whole restricted domain is covered.

For each direction u, $u = 1, 2, \cdots, n$, the new step vector component $\boldsymbol{\gamma}'_u$ is

$$\gamma'_u = \begin{cases} \gamma_u \left(1 + \zeta \frac{M_{a_u}/M_t - 0.6}{0.4}\right) & \text{if} \quad M_{a_u} > 0.6 M_t, \\ \dfrac{\gamma_u}{1 + \zeta \frac{0.4 - M_{a_u}/M_t}{0.4}} & \text{if} \quad M_{a_u} < 0.4 M_t, \\ \gamma_u & \text{otherwise} \end{cases} \tag{16}$$

where ζ is a constant parameter that controls the step variation along each u^{th} direction. The aim of these variations in step length is to maintain the average percentage of accepted moves M_a at about one-half of the total number of moves M_t, both for a same value of T. [26, 27, 28] give a more detailed discussion about it.

The values of the objective function for $\boldsymbol{\rho}'$ and $\boldsymbol{\rho}_i$ configurations denoted as $F(\boldsymbol{\rho}_i)$ and $F(\boldsymbol{\rho}')$ are calculated through Eq. (14). In the minimization problem, if

$$\Delta F = F(\boldsymbol{\rho}') - F(\boldsymbol{\rho}_i) < 0 \quad \text{(i.e., } \boldsymbol{\rho}' \text{ is better)} \tag{17}$$

then, the new movement is accepted, otherwise, it is accepted with a probability $P(i)$

$$P(i) = exp\left(-\frac{\Delta F}{T_i}\right) \tag{18}$$

where T_i is the control parameter (temperature) in the i^{th} iteration.

The EIT forward problem is used to calculate $\boldsymbol{V_c}(\boldsymbol{\rho})$ that, through Eq. (14), is part of Eq. (17). This means that for each transition in the space of solutions Eq. (11) is solved first to get $\boldsymbol{v_c}(\boldsymbol{\rho})$, then, it is calculated $F(\boldsymbol{\rho})$ based on Eq. (14). After this, the metropolis criterion is used to accept or reject a new configuration, as mentioned above.

After $(N_t * n)$ iterations, it is changed the value of T according to the chosen annealing function and the cooling factor α as defined in Eq. (13), and a new step vector $\boldsymbol{\gamma}$ is calculated by the Eq. (16).

5. METHODOLOGY AND TESTS

5.1 numerical phantom

A numerical phantom was used to simulate the data acquired by an EIT system. The data was used to test the image reconstruction algorithm. The phantom is FEM discretized domain, whose distribution of resistivity $\boldsymbol{\rho}^*$ is chosen. It allows to get the electrical potentials $\boldsymbol{V_m}$ in $\partial\boldsymbol{\Omega}$ through the l electrodes for each one of the p injected current patterns. That is, to find the electrical potentials in the electrodes the forward problem for each p injected current patterns is solved by Eq. (11) and the vector $\boldsymbol{v_m}$ contains only the electrodes electrical potentials. Then, these electrical potentials are used for the image estimation through the implemented SA algorithm which is compared with the image of resistivity distribution $\boldsymbol{\rho}^*$ chosen for the numerical phantom.

The algorithm for solving the inverse problem in both, numerical and experimental tests, is implemented using C language and the FE meshes are generated by Gmsh on a Linux operational system. In order to avoid inverse crimes, the mesh used in the phantom domain must have more elements than the mesh used to solve the inverse problem.

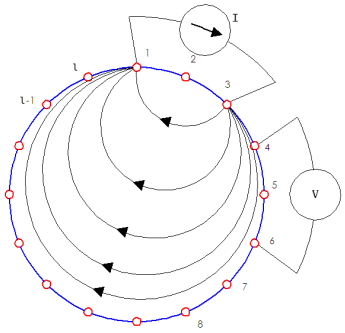

Figure 1. Adopted method for injecting currents and reading electrical potentials

5.2 Numerical data tests

The aim of the numerical data tests is to identify an stable algorithm to be used with experimentally obtained data. All tests are made with a circular domain of 300 mm of diameter and the object is also circular with diameter of 60 mm. The injected current is 2mA, bipolar and the method shown in Fig. 1 (this figure corresponds to one current load case) is adopted for injecting currents and reading electrical potentials.

5.2.1 Test 1

For solving the forward problem with the numerical phantom the domain is discretized by 222 nodes, 362 2-D triangular elements and 16 electrodes and the resistivity value of the background is 17Ωm. The resistivity value of the object (target) is 1000Ωm. The finite elements mesh used to solve the inverse problem has 122 nodes, 170 elements and 16 electrodes. Figure 2(a) shows the image that will be reconstructed, the background (blue) and target (red) regions, and Fig. 2(b) presents the finite elements mesh of the inverse problem. The initial temperature T_0 is 0.05, the cooling factor α is 0.8, stopping criterion is 40 iterations, the number of iterations at each temperature N_t is 15, the parameter ζ that controls the step variation is 1, the resistivity values are between 17Ωm and 1000 Ωm and the initial value for resistivity distribution of the domain $\boldsymbol{\rho}_0$ is 20Ωm and 0.02Ωm^2 for the electrode parameters.

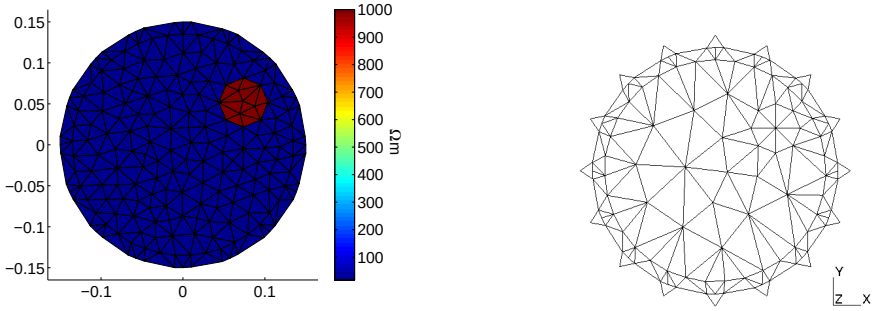

(a) (b)

Figure 2. (a) requested original image and (b) FE mesh of inverse problem to test 1.

5.2.2 Test 2

The aim of this test is to check whether the algorithm identifies that the object was moved to a different region. The resistivity value of the background is 10Ωm and for the target region is 500Ωm. For solving the forward problem with the numerical phantom the domain is discretized by 547 nodes, 980 elements and 16 electrodes. The finite elements mesh used to solve the inverse problem has 229 nodes, 344 elements and 16 electrodes. Figure 3(a) shows the image that will be reconstructed, the background (blue) and target (red) regions, and Fig. 3(b) presents the finite elements mesh of the inverse problem. T_0 is 100, α is 0.9, stopping criterion is 20 iterations, N_t is 30, ζ is 2, the resistivity limits are between 10Ωm and 600 Ωm and $\boldsymbol{\rho}_0$ is 12Ωm and 0.02Ωm^2 for the electrodes.

5.3 Experimental data tests

The procedure for the experimental data tests is similar to the used for the numerical data, except that the electrical potentials $\boldsymbol{V_m}$ where measured. A current source injected 2 mA peak sinusoidal current of 125 kHz on pair of electrodes.

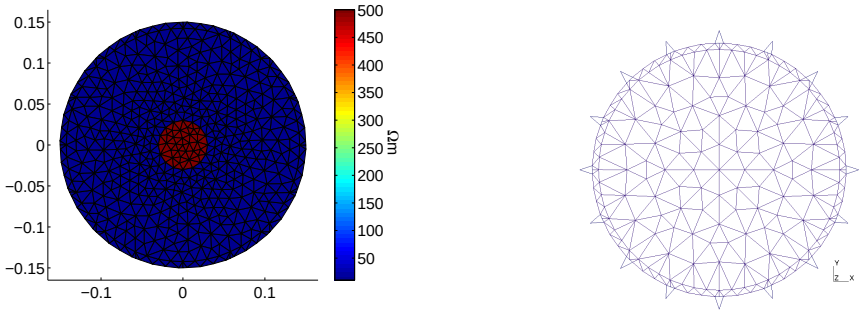

(a) (b)

Figure 3. (a) requested original image and (b) FE mesh of inverse problem to test 2

The electrodes were attached to the boundary of a cylindrical container with 300mm of inner diameter containing a 0.3 g/L saline solution (NaCl). Its resistivity is approximately 17Ωm. The currents are injected and electrical potentials are measured through a data acquisition board, following the current patterns represented in Fig. 1. The aim of these tests is to identify a circular glass object with 32mm of diameter and resistivity equal to $10^6\Omega$m approximately, which is immersed into the container. The 30 electrodes are rectangular with 35mm high and 10mm wide.

5.3.1 Test 3

The object was positioned at the center of container as shown in Fig. 4(b). The FE mesh used for the inverse problem has 409 nodes, 636 elements and 30 electrodes (see Fig. 4(a)). The test was run using T_0 equal 5, α equal 0.99, maximum number of iterations equal 50 iterations, N_t equal 30, ζ equal 1, the resistivity limits equal 10Ωm and 200 Ωm, $\boldsymbol{\rho}_0$ equal 25Ωm and electrode parameters equal $0.02\Omega\text{m}^2$.

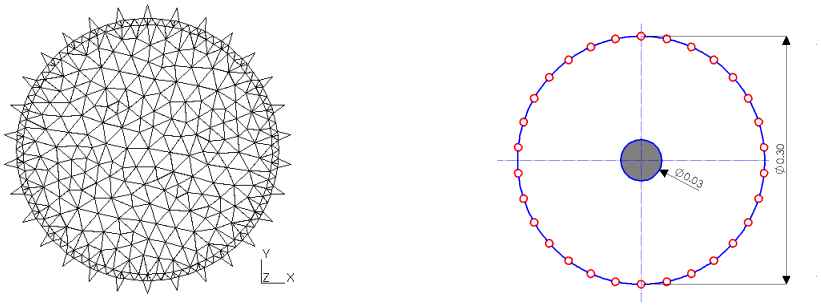

(a) (b)

Figure 4. (a) FE mesh for the inverse problem and (b) used configuration for test 3

6. RESULTS

Figures 5(a), 5(b), 6(a) and 6(b) show images and the objective function histories obtained by SA algorithm for the test 1 and 2. In tests 1 and 2 the position and size of the virtual object were recovered properly and the amplitude reached the expected value (both basal and perturbed region). However, due to the not very refined meshes and to the difficulty to tune the SA parameters some elements did not reach the upper limit. For test 1 the elapsed time was 468 minutes and final objective function was 0.48, and for test 2 was 605 minutes and the final objective function was 0.0015. The objective function of test 2 converged faster than the one of test 1.

Figures 7(a) and Fig. 7(b) show image and the objective function history obtained by SA algorithm for the test 3. The position of the object was recovered properly but its diameter resulted bigger than expected, it is probably related to the poorly refined mesh and lack of accurate *prior* information. The region of higher resistivity was identified but some elements around this region (that would not have) acquired a resistivity value higher than expected one. However due to the discretization and to the difficulty to tune the SA parameters not all of elements reached the upper limit. The elapsed time was 503 minutes and final objective function was 6.35.

7. CONCLUSIONS

An EIT algorithm based on SA method was implemented for image estimation. With numerical data good results were obtained. The feasibility of the algorithm was demonstrated. The performance of the algorithm when using experimental

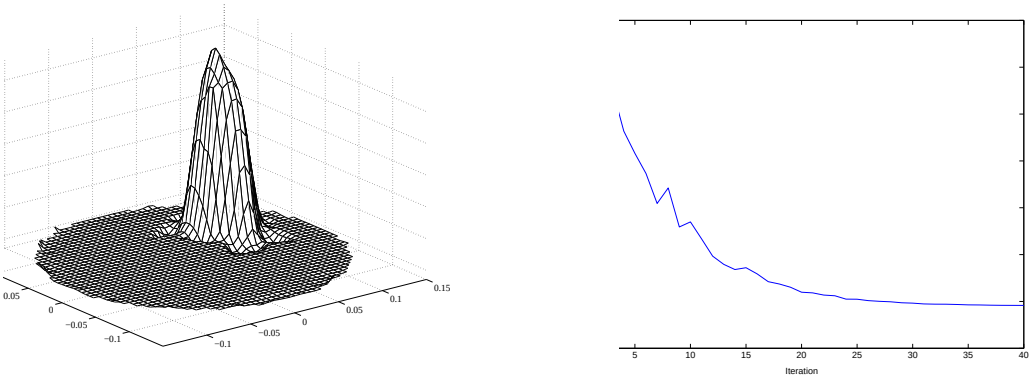

(a) (b)

Figure 5. (a) FE mesh for the inverse problem and (b) used configuration for test 1

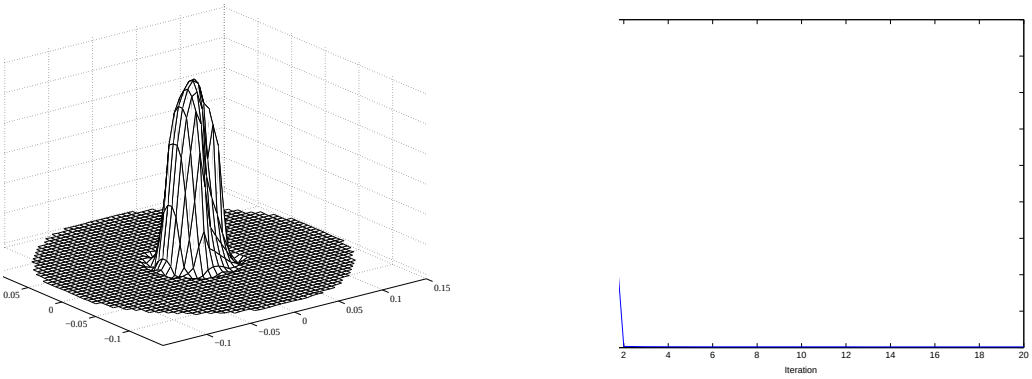

(a) (b)

Figure 6. (a) FE mesh for the inverse problem and (b) used configuration for test 2

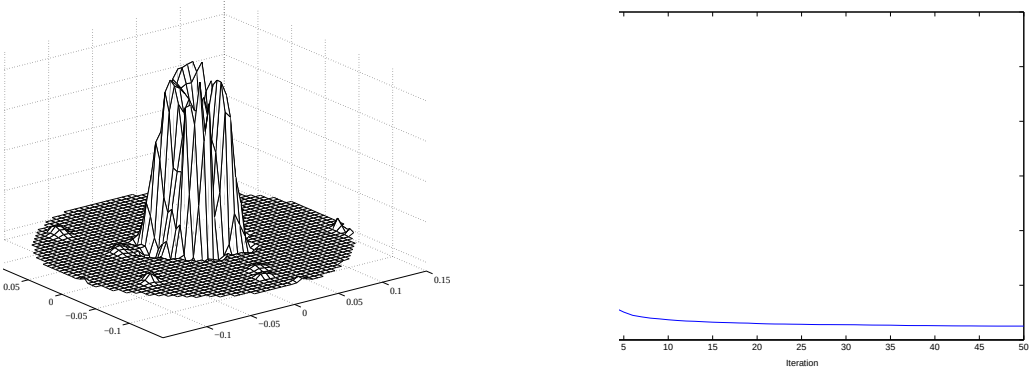

(a) (b)

Figure 7. (a) FE mesh for the inverse problem and (b) used configuration for test 3

data was good because the algorithm identified the higher resistivity region although the mesh has poor discretization. The SA algorithm allows to include restrictions to the solution space and introducing *prior* information without using classicalregularization techniques. The processing time is high and future works will attempt to diminish the processing time. The spatial resolution of the image may improve through the introduction of *prior* information, for instance, through the use of an anatomical atlas, and the use of more refined meshes.

8. ACKNOWLEDGMENT

First author thanks the financial support of FAPESP through master scholarship with process number $04/11159 - 1$.

9. REFERENCES

Barber, D.C., Brown, B.H., 1984, "Applied Potential Tomography", Journal of Physics E:Scientific Instruments, Vol.17, pp. 723-733.

Cheney, M., Isaacson, D. and Newell, J.C. and Goble, J. and Simske, S., 1999, "Electrical Impedance Tomography", SIAM Journal on Applied Mathematics, Vol.41, No. 1, pp. 85-101.

Harris, N.D, Sugget, A.J. and Barber, D.C. and Brown, B.H., 1987, "Applications of applied potential tomography (APT) in respiratory medicine", Clin. Phys. Physiol. Meas., Vol.8, pp. 155-165.

Holder, D., 1993, "Clinical and Physiological Applications of Electrical Impedance Tomography", Londres: UCL Press, Vol.8, 310 p.

Akbarzadeh, M.R., Tompkins, W.J. and Webster, J.G., 1990, "Multichannel Impedance Pneumography For Apnea Monitoring", Proceedings of the Twelfth Annual International Conference of the IEEE Engineering in Medicine and Biology Society, Vol.12, No. 3, pp. 1048-1049.

Bagshaw, A.P., Liston, A.D. and Bayford, R.H. and Tizzard, A. and Gibson, A.P. and Tidswell, A.T. and Sparkes, M.K. and Dehghani, H. and Binnie, C.D. and Holder, D.S., 2003, "Electrical impedance tomography of human brain function using reconstruction algorithms based on the finite element method", NeuroImage, Vol.20, pp. 752-764.

Noordegraaf, A.V., Faes, T.J. and Janse, A. and Marcus, J.T. and Bronzwaer, J.G. and Postmus, P.E. and de Vries, P.M., 1997, "Noninvasive assessment of right ventricular diastolic function by electrical impedance tomography", CHEST, Vol.111, pp. 1222-1228.

Cherepenin, V., Karpov, A. and Korjenevsky, A. and Kornienko, V. and Kultiasov, Y. and Ochapkin, M. and Trochanova, O. and Meister, D., 2002, "Three-dimensional EIT imaging of breast tissues: system design and clinical testing", IEEE Trans. Medical Imaging, Vol.21, No. 6, pp. 662-667.

Barber, D.C., 1990, "Quantification in impedance imaging", Clin. Phys. Physiol. Meas., Vol.11, pp. 45-56.

Asfaw, Y.W., 2005, "Automatic detection of detached and erroneous electrodes in Electrical Impedance Tomography", School of Information Technology and Engineering, University of Ottawa.

Murai, T., Kagawa, Y., 1985, "Electrical Impedance Computed Tomography based on a finite element model" , IEEE Transactions on Biomedical Engineering, Vol.32, No. 3, pp. 177-184.

Kallman, J.S., Berryman, J.G., 1992, "Weighted least-squares criteria for electrical impedance tomography", IEEE Trans. Medical Imaging, Vol.11, pp. 284-292.

Calderón, A.P., 1980, "On an Inverse Boundary Value Problem", Proceedings of Seminar on Numerical Analysis and its Applications to Continuum Physics, Brazil: Soc. Brasileira de Matemática, pp. 65-73.

Connolly, T.J., Wall, D.J.N., 1998, "On an inverse problem, with boundary measurements for the steady state diffusion equation", Inverse Problems, Vol.4, pp. 995-1012.

Kim, Y., Webster, J.G. and Tompkins, W.J., 1983, "Electrical impedance imaging of the thorax", Journal of Microwave Power, Vol.18, pp. 245-257.

Yorkey, T.J., Webster, J.G. and Tompkins, W.J., 1987, "Comparing Reconstruction Algorithms for Electrical Impedance Tomography", IEEE Trans. on Biomed. Eng., Vol.34, No. 11, pp. 843-852.

Adler, A., Guardo, R., 1996, "Electrical Impedance Tomography: Regularized imaging and Contrast Detection", 1996, IEEE Trans. Medical Imag., Vol.15, pp. 170-179.

Metropolis, N., Rosenbluth, A.W. and Rosenbluth, M.N. and Teller, A.H. and Teller, E., 1953, "Equation of state calculation by fast computing machines", Journal of Chemistry Physics, Vol.21, pp. 1087-1091.

Lutfiyya, H., McMillin, B. and Poshyanonda, P. and Dagli, C., 1992, "Composite Stock Cutting Through Simulated Annealing", Mathematical and Computer Modelling, Vol.34, pp. 111-124.

Hua, P., Woo, J. and Webster, J.G. and Tompkins, W., 1993, "Finite element modeling of electrode-skin contact impedance in Electrical Impedance Tomography", IEEE Transactions on Biomedical Engineering, Vol.40, No. 4, pp. 335-343.

Cheng, K.S., Isaacson, D. and Newell, J.C. and Gisser, D.G., 1989, "Electrode models for electric current computed tomography", IEEE Trans Biomed Eng., Vol.36, No. 9. pp. 918-924.

Logan, D.H., 1986, "A First Course in the Finite Element Methods", Boston: PWS Engineering.

Kirkpatrick, S., Gellat, C.D. and Vecchi, M.P., 1983, "Optimization by Simulated Annealing", Science, Vol.220, pp. 671-680.

Cerny, V., 1985, "Thermodynamical aproach to the traveling salesmanproblem: an efficient simulation algorithm", Journal of Optimization Theory and Applications, Vol.45, No. 1, pp. 41-51.

Elliott, S.J., 2001, "Signal Processing for Active Control", Academic Press Inc., 511 p.

Corana, A., Marchesi, M. and Martini, C. and Ridella, S., 1987, "Minimizing Multimodal Functions of Continuous Variables with the Simulated Annealing Algorithm", ACM Transactions on Mathematical Software, Vol.13, pp. 262-280.

Vanderbilt, D., Louie, S.G., 1984, "A Monte Carlo Simulated Annealing Approach to Optimization over Continuous Variables", Journal of Comput. Phys., Vol.56, pp. 259-271.

Bohachewsky, I.O., Johnson, M.E. and Stein, M.L., 1986, "Generalised simulated annealing for function optimization", Technometrics, Vol.28, pp. 209-217.

10. Responsibility notice

The author(s) is (are) the only responsible for the printed material included in this paper.